Biomech Model Mechanobiol (2011) 10:779–787
DOI 10.1007/s10237-010-0273-z

ORIGINAL PAPER

A 3D active-passive numerical skeletal muscle model incorporating initial tissue strains. Validation with experimental results on rat tibialis anterior muscle

J. Grasa · A. Ramírez · R. Osta · M. J. Muñoz · F. Soteras · B. Calvo

Received: 2 July 2010 / Accepted: 16 November 2010 / Published online: 3 December 2010

Abstract This paper presents a three-dimensional finite element model of skeletal muscle and its validation incorporating inital tissue strains. A constitutive relation was determined by using a convex free strain energy function (SEF) where active and passive response contributions were obtained fitting experimental data from the rat tibialis anterior (TA) muscle. The passive and active finite strains response was modelled within the framework of continuum mechanics by a quasi-incompressible transversely isotropic material formulation. Magnetic resonance images (MRI) were obtained to reconstruct the external geometry of the TA. This geometry includes initial strains also taken into account in the numerical model. The numerical results show excellent agreement with the experimental results when comparing reaction force-extension curves both in passive and active tests. The proposed constitutive model for the muscle is implemented in a subroutine in the commercial finite element software package ABAQUS.

Keywords Passive and active behaviour of skeletal muscle tissue · Muscle initial strains · Hyperelasticity

J. Grasa (✉) · A. Ramírez · B. Calvo
Group of Structural Mechanics and Materials Modelling, Aragón Institute of Engineering Research, University of Zaragoza, Zaragoza, Spain
e-mail: jgrasa@unizar.es

J. Grasa · A. Ramírez · B. Calvo
CIBER-BBN, Centro de Investigación Biomédica en Red en Bioingeniería, Biomateriales y Nanomedicina, Zaragoza, Spain

R. Osta · M. J. Muñoz · F. Soteras
Lagenbio-Ingen, Aragón Institute of Engineering Research, University of Zaragoza, Zaragoza, Spain

1 Introduction

Skeletal muscle is a biological soft tissue whose main task is body motion. Apart from thinking, every human activity requires a movement, or at least a muscle contraction (MacIntosh et al. 2006). For this reason, muscles are as diverse as the movements they perform.

In spite of shape and function differences, skeletal muscle can be considered as a network of muscle fibres (contractile element) surrounded, at different levels, by connective tissue (elastic element) that passively resists muscle stretching. It is well known that muscle fibres also contribute to passive behaviour (series elastic element) (Hill 1938; Magid and Law 1985). Connective tissue consists of collagen and elastin fibres embedded in an amorphous ground substance organized in three anatomical parts: the epimysium, perimysium and endomysium (Borg and Caulfield 1980). All these parts play an important role in the lateral transmission of the force produced within muscle fibres (Arruda et al. 2007) and also for blood and nervs supply.

Advances in numerical methods, medical imaging and experimental testing of biological tissues now allow the assessment of three-dimensional (3D) models for evaluating strain and stress fields within living tissues. FE models that include 3D geometric representations of muscles coupled with mathematical descriptions of their complex material behaviour have been widely developed by various researchers (Blemker and Delp 2005; Fernandez and Hunter 2005). For obtaining these numerical models, some simplifications of the physical problem have to be taken into account. Usually, mechanical properties for the input material parameters are based on "in vitro" measurements (Martins et al. 1998), stimations (Oomens et al. 2003) or adapted from cardiac muscle (Fernandez et al. 2005). Sometimes external geometry is obtained from idealized muscles (Johansson et al. 2000;

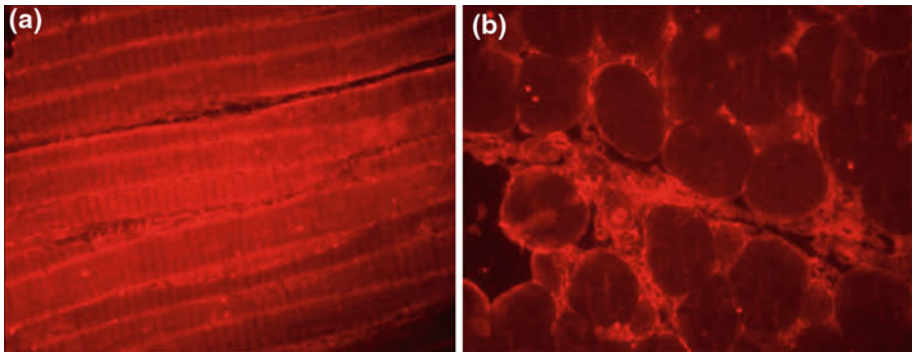

Fig. 1 Picrosirius *red* staining for TA collagen I (**a**) Longitudinal section (**b**) Transversal section

Yucesoy et al. 2002; Tsui et al. 2004; Böl and Reese 2008; Chi et al. 2010) or based on real muscles with simplifications (Oomens et al. 2003; Blemker et al. 2005). Given this situation, extra efforts are necessary in these cases to ensure that the finite element model is reliable. The predicted solution should be correctly interpreted and validated before it is considered to have any clinical value.

This work presents the development of a validated 3D FE model of the rat TA muscle capable of simulating contractions in healthy conditions, including experimentally fitted constitutive models for muscle and tendon tissue, an accurate geometry and appropiate experimental procedures to be validated. We have created in this way a 3D finite element mesh of the TA based on MR images. To define constitutive material laws, the formulations proposed in previous works for passive behaviour (Calvo et al. 2010) and active behaviour (Ramírez et al. 2010) have been implemented into the commercial FE software ABAQUS (Hibbit et al. 2006). Furthermore, because MR images were obtained "in vivo", the model incorporates initial tissue strains. This fact is reflected in the laboratory when tissue is released showing a significant change in external geometry (Gardiner et al. 2001). Due to the non-linear behaviour of this kind of tissue, an erroneous inclusion of the initial strain state in computational models can lead to serious errors (Peña et al. 2006).

We describe the validation of this model simulating a controlled passive stretch of the whole muscle-tendon unit "in vivo". Moreover, the active contribution for muscle contraction was validated again from "in vivo" experimental tests, in this case, of isometric contraction.

2 Model formulation

From a mechanical point of view, muscles can be considered as composite materials made of long cells (muscular fibres) surrounded by connective tissue i. e., collagen and elastin fibres embedded in an amorphous ground substance (MacIntosh et al. 2006). The preferential direction defined by the family of collagen fibres is supposed to be aligned in the direction of muscle fibres for fusiform-shaped muscles (Martins et al. 1998; Blemker and Delp 2005; Tang et al. 2009). As can be seen in Fig. 1, collagen type I, which transmits the main part of passive muscle force (Arruda et al. 2007), surrounds muscle fibres, and lies in the same way, longitudinally. For tendon tissue, the same reasoning for its behaviour, related mainly to connective tissue, can be assumed.

Skeletal muscle and tendon are supposed to be hyperelastic and transversely isotropic under finite strains (Weiss et al. 1996; Martins et al. 1998; Oomens et al. 2003; d'Aulignac et al. 2005; Calvo et al. 2010). Under this assumption, the constitutive strain energy function for these materials depends on the direction of the family of fibres (collagen and muscular) at a point $\mathbf{X}$ that is defined by the unit vector field $\mathbf{m}_0$. The stretch λ, defined as the ratio between the length of the fibre in the deformed and reference configurations, can be expressed as $\lambda^2 = \mathbf{m}_0 \cdot \mathbf{C}\mathbf{m}_0 = I_4$ with $\mathbf{C}$ being the right Cauchy-Green strain measure $\mathbf{C} = \mathbf{F}^{\mathbf{T}}\mathbf{F}$, being $\mathbf{F}$ the deformation gradient $\mathbf{F} = \frac{\partial \mathbf{x}}{\partial \mathbf{X}}$ with $\mathbf{x}$, $\mathbf{X}$ the coordinates of each point in the current and initial configurations respectively.

Due to the well-known difficulties involved in displacement-based finite elements in the analysis of nearly incompressible materials (Holzapfel 2000), we postulated a multiplicative decomposition of $\mathbf{F} = J^{1/3}\bar{\mathbf{F}}$ and $\mathbf{C} = J^{2/3}\bar{\mathbf{C}}$ into volume-changing (dilational) and volume-preserving (distortional) parts, with $J = det\mathbf{F}$. To characterize isothermal processes, we postulate the existence of a unique decoupled representation of the SEF Ψ that could be expressed as:

$$\Psi = \Psi_{\text{vol}}(J) + \bar{\Psi}_p(\bar{I}_1, \bar{I}_2, \bar{I}_4) + \bar{\Psi}_a(\sigma_0, \bar{\lambda}, f_r, t) \qquad (1)$$

where $\Psi_{\text{vol}} = 1/D(J-1)^2$, $\bar{\Psi}_p$ and $\bar{\Psi}_a$ are the strain energy densities associated with the volumetric, passive and active responses, respectively. These last two functions are described below.

(a) Passive behaviour.
The SEF for the passive contribution of TA muscle was proposed in a previous work (Calvo et al. 2010) based

Table 1 Material model parameters for muscle and tendon passive behaviour

	c_1	c_3	c_4	c_5	c_6	c_7	$\bar{I}_{4_0}$	$\bar{I}_{4_{\text{ref}}}$
$\text{Muscle}_{\text{mean curve}}$	0.001	0.053915	0.782802	5.742780	−9.035709	−4.875961	1.254400	3.189796
$\text{Muscle}_{\text{mean parameters}}$	0.008837	0.009877	2.237879	3.063670	−4.759628	−2.763531	1.256385	2.472600
$\text{Tendon}_{\text{mean curve}}$	0.01	0.054292	6.860021	57.738461	−66.243575	−57.078409	1.0	1.44
$\text{Tendon}_{\text{mean parameters}}$	0.0810	0.045038	7.570983	58.007323	−66.682665	−57.328411	1.0	1.445060

Constant values in MPa (Calvo et al. 2010)

on "in vitro" uniaxial experimental tests and takes the form:

$$\begin{aligned}
&\bar{\Psi}_p = c_1(\bar{I}_1 - 3) + \bar{\Psi}_f \\
&\bar{\Psi}_f = 0 \qquad \bar{I}_4 < \bar{I}_{4_0} \\
&\bar{\Psi}_f = \frac{c_3}{c_4}(\exp^{c_4(\bar{I}_4 - \bar{I}_{4_0})} - c_4(\bar{I}_4 - \bar{I}_{4_0}) - 1) \\
&\quad \bar{I}_4 > \bar{I}_{4_0} \quad \text{and} \quad \bar{I}_4 < \bar{I}_{4_{\text{ref}}} \\
&\bar{\Psi}_f = c_5\sqrt{\bar{I}_4} + \frac{1}{2}c_6 \ln(\bar{I}_4) + c_7 \qquad \bar{I}_4 > \bar{I}_{4_{\text{ref}}}
\end{aligned} \tag{2}$$

where $\bar{I}_1$ represents the first modified invariant of the modified right Cauchy-Green strain tensor, $\bar{I}_4 > \bar{I}_{4_0}$ characterizes the mechanical response on the collagen fibre direction and $\bar{I}_{4_{\text{ref}}}$ characterizes the stretch at which collagen fibres start to be straightened. $c_1 > 0$, $c_3 > 0$, $c_5 > 0$ and $c_6 < 0$ are stress-like parameters, $c_4 > 0$ is a dimensionless parameter and c_7 is a strain energy parameter. Table 1 shows values of these paremeters for the muscle-tendon unit.

(b) Active behaviour.

The SEF, $\bar{\Psi}_a$, in Eq. (1) allows us to incorporate the active mechanical response of the tissue and takes the form (Ramírez et al. 2010):

$$\bar{\Psi}_a = \sigma_0 \eta(\bar{\lambda}) \gamma(f_r, t) \tag{3}$$

where σ_0 is the maximum tensile stress generated by the muscle, the function $\eta(\bar{\lambda})$ represents the effective overlap between the filaments in the contractile element taking values between 0 and 1 and $\gamma(f_r, t)$ is the activation function. As mentioned previously, the model was validated by means of isometric tests, so $\bar{\Psi}_a$ does not depend on stretch velocity.

Several expressions have been proposed by different authors for $\eta(\bar{\lambda})$ (Blemker et al. 2005; Böl and Reese 2008). In this work, a sigmoid function that presents a good fit to experimental data is proposed:

$$\eta(\bar{\lambda}) = e^{\frac{-(\bar{\lambda} - \lambda_{\text{opt}})^2}{2(1-\beta)^2}} \tag{4}$$

Table 2 Material model parameters for muscle active behaviour (Ramírez et al. 2010)

σ_0 (MPa)	λ_{opt}	β	T' (s)	P' (N)	t_i (s)	r	c
0.8	1	0.83616	0.04	0.11	0.01667	1.0535	1.1245

λ_{opt} is the optimum muscle stretch, $\bar{\lambda}$ is the actual stretch and β corresponds to the curvature of the sigmoid function.

The activation function $\gamma(f_r, t)$ proposed is:

$$\gamma(f_r, t) = \sum_{i=1}^{n} \left[\left(1 - re^{(f_r T')/c}\right) \left(P' \frac{t - t_i}{T'} e^{1-(\frac{t-t_i}{T'})} \right) \right] \tag{5}$$

where T' is the apparent contraction time for all muscle generated by a pulse of the excitation signal and P' is the apparent amplitude force generated, t_i is the time interval between stimuli, that is $1/f_r$, r determines the ratio of twitch and tetanus stress, c is the rate of increase in force with increasing frequency and n is the number of stimulation pulses. Table 2 shows all these parameters, obtained from "in vivo" experimental tests (Ramírez et al. 2010).

With the SEF, the constitutive equation for compressible hyperelastic materials can be defined from the Clausius-Planck inequality as:

$$\begin{aligned}
\mathbf{S} &= \frac{\partial \Psi}{\partial \mathbf{C}} = \frac{\partial \Psi_{\text{vol}}(J)}{\partial \mathbf{C}} + \frac{\partial \bar{\Psi}_p(\bar{\mathbf{C}})}{\partial \mathbf{C}} + \frac{\partial \bar{\Psi}_a(\bar{\mathbf{C}})}{\partial \mathbf{C}} \\
&= \mathbf{S}_{\text{vol}} + \bar{\mathbf{S}}_p + \bar{\mathbf{S}}_a
\end{aligned} \tag{6}$$

The associated decoupled elasticity tensor may be written as:

$$\mathbb{C} = \mathbb{C}_{\text{vol}} + \bar{\mathbb{C}}_p + \bar{\mathbb{C}}_a = 2\frac{\partial \mathbf{S}_{\text{vol}}}{\partial \mathbf{C}} + 2\frac{\partial \bar{\mathbf{S}}_p}{\partial \mathbf{C}} + 2\frac{\partial \bar{\mathbf{S}}_a}{\partial \mathbf{C}} \tag{7}$$

The true Cauchy stress tensor $\boldsymbol{\sigma}$ and the elasticity tensor in the spatial description $\mathbb{c}$ were obtained in a standard manner for compressible hyperelastic materials, see eg. Weiss et al. (1996) or Holzapfel (2000) as $1/J$ times the pushforward of

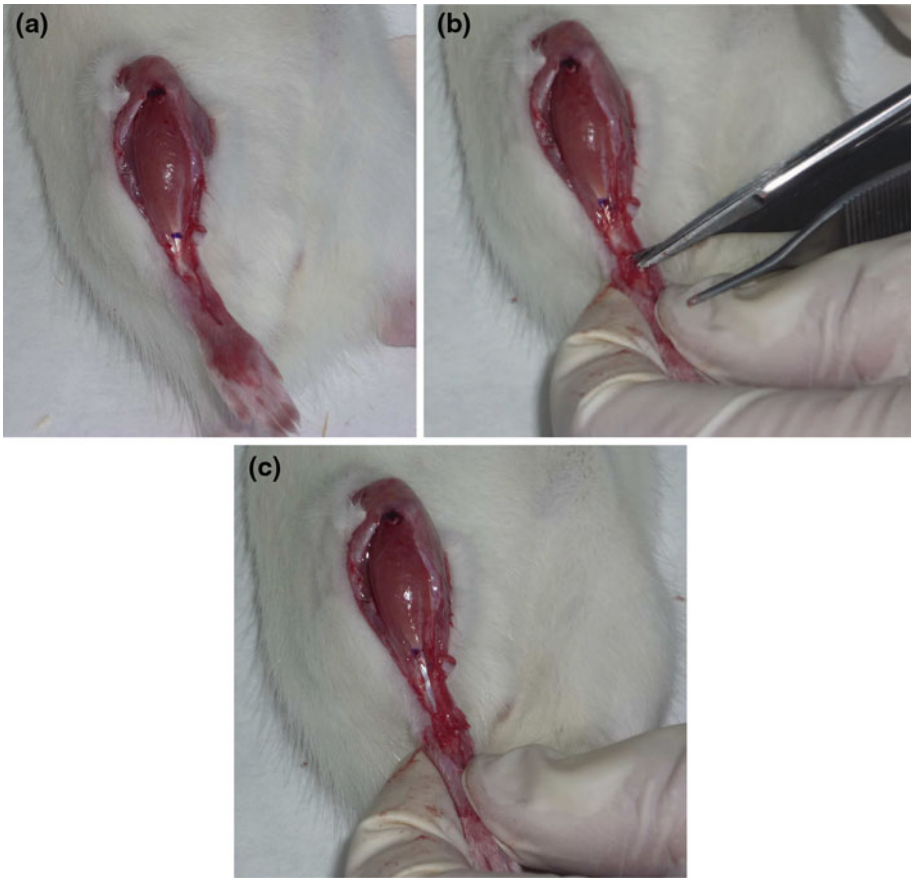

Fig. 2 Evaluation of initial strains by cutting distal insertion: **a** reference configuration, **b** during the cutting, **c** stress-free configuration

$\bar{\mathbf{S}}$ or c, respectively:

$$\boldsymbol{\sigma} = J^{-1}\boldsymbol{\chi}_*(\mathbf{S}) \qquad \mathbb{c} = J^{-1}\boldsymbol{\chi}_*(\mathbb{C}) \tag{8}$$

This constitutive model was implemented in the commercial FE code ABAQUS v.6.9 (Hibbit et al. 2006) through a Fortran UMAT user subroutine.

2.1 Initial strain

Biological soft tissues are usually exposed to a complex distribution of "in vivo" initial strains. This state is a consequence of the continuous growth, remodelling, damage and viscoplastic strains that these living materials suffer throughout their whole lives. Initial strains can be relieved by selective cutting of the living tissue and removal of its internal constraints (see Fig. 2).

In order to describe the current deformation state, we followed the methodology proposed by Gardiner and Weiss (2003) to enforce initial strains in hyperelastic soft tissues. Three different configurations were defined: (a) the stress-free state (Ω_{sf}), (b) the reference state in which the material is only under the initial strain (Ω_0) and (c) the current deformed state (Ω). It was assumed that the total deformation gradient tensor corresponding to the current state $\mathbf{F}$ admits a multiplicative decomposition $\mathbf{F} = \mathbf{F}_r\mathbf{F}_0$, where, $\mathbf{F}_0$ represents the deformation gradient corresponding to the initial strains and $\mathbf{F}_r$ is the deformation gradient that results from applying the external loads to this initial configuration Ω_0.

As $\mathbf{F}_0$ is difficult to determine from experiments, we assume that $\mathbf{F}_0$ corresponds to an axial stretch λ_0 along the fibre direction $\mathbf{m}_0$ in the reference state Ω_0 (Gardiner and Weiss 2003). In a coordinate system $(^*)$ where the muscle fibre direction $\mathbf{m}_0$ is aligned with the X_1 axis, $\mathbf{F}_0$ can be written as:

$$\left[\mathbf{F}_0^*\right] = \begin{bmatrix} \lambda_0 & 0 & 0 \\ 0 & \frac{1}{\sqrt{\lambda_0}} & 0 \\ 0 & 0 & \frac{1}{\sqrt{\lambda_0}} \end{bmatrix} \tag{9}$$

and transformed to the global system:

$$\mathbf{F}_0 = \mathbf{R}\mathbf{F}_0^* \tag{10}$$

with $\mathbf{R}$ being the rotation tensor taken from this local system and applied to the global one (Peña et al. 2006).

The total stresses corresponding to the current state $\boldsymbol{\sigma}_r$ are obtained in the standard form using the SEF $\Psi_{\Omega_{\text{sf}}}$ through $\mathbf{F}_r$.

Fig. 3 Generation of "in vivo" MR image of a female Wistar adults rat

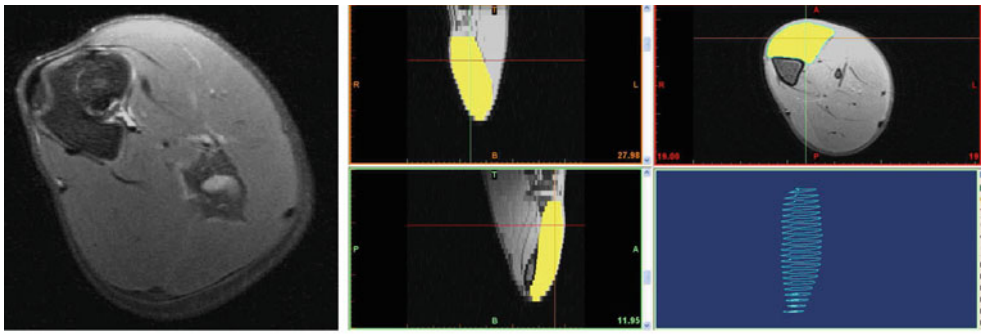

(a) MR images **(b)** Segmentation with Mimics

Fig. 4 MR images of the rat leg and segmentation

$$\boldsymbol{\sigma}_r = \frac{2}{J_r}\boldsymbol{\chi}_{*r}\left[\frac{\partial \Psi_{\Omega_{\mathrm{sf}}}(\mathbf{C})}{\partial \mathbf{C}}\right] = \frac{2}{J_r}\mathbf{F}_r^{-1}\left[\frac{\partial \Psi_{\Omega_{\mathrm{sf}}}(\mathbf{C})}{\partial \mathbf{C}}\bigg|_{\mathbf{C}=\mathbf{C}_r}\right]\mathbf{F}_r^{-T} \tag{11}$$

with $J_r = J_0 J$.

3 Finite element model of tibial anterior

We reconstructed the surface geometry of the tibialis anterior muscle from MR images of a female Wistar adult rat with a body mass of 215 ± 15 g. MR images were obtained with a Bruker BioSpin of 7 T. Rats were anaesthetised with an intraperitoneal injection of pentobarbital sodium solution (30 mg/kg). The experiment was approved by the Autonoma University of Barcelona Ethics Committee for the use of animals in experimentation.

Images were taken from the distal femoralis condilus to metatarsian. The rat was placed in a supine position with the right hind limb extended as can be observed in Fig. 3. Thirty scans (512×512 pixels) along muscle length were obtained with a resolution of 0.06 mm/pixel.

The axial images were used to achieve a detailed reconstruction of the TA muscle anatomy (see Fig. 4). On each image, we manually outlined the boundary of the muscle of interest and a three-dimensional polygonal surface model was generated from the set of two-dimensional outlines using Mimics software (Materialise 2010).

We created solid hexahedral meshes of the muscle and tendon from the surface model using the finite element mesh generator ABAQUS (Hibbit et al. 2006). Figure 5a shows the three-dimensional finite element model of the tibialis anterior muscle. We also generated two representation of the fibre geometry: in the first case, the fibres were defined in the longitudinal direction (z axis) and in the second case, the fibres followed the outline of fusiform muscle geometry (see Fig. 5b).

It is important to note that the MR images correspond to TA muscle obtained "in vivo", that is, in the physiological configuration. For this reason, the muscle tissue is subjected to an initial strain state, $\mathbf{F}_0$ that must be taken into account in the numerical model. Moreover, the fascia layer has not been considered in the model because it was removed in all the experimental tests to isolate the muscle tissue correctly.

4 Results

In this section, some key results are presented to validate the numerical model. The results are grouped into three sections. First, the effect of initial strains is included in the mesh. Second, uniaxial passive tensile tests of the whole muscle-tendon unit are presented and compared with the numerical simulation. Finally, the validation of the active behaviour

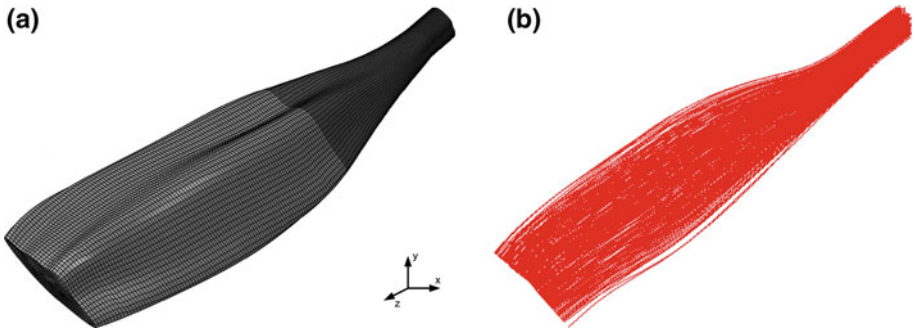

Fig. 5 Finite element model of the reference configuration (Ω_0) and fibre orientation of the rat tibialis anterior muscle

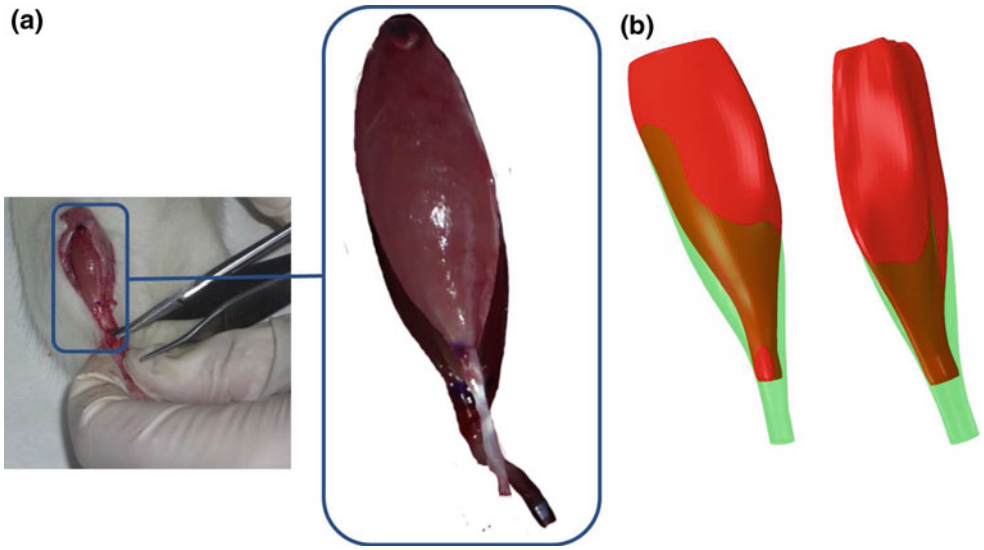

Fig. 6 Initial strains. **a** After cutting off the distal tendon, the muscle shortens as can be observed in the superimposed images. **b** Finite element simulation of this effect, stress-free state in the *red mesh* (Ω_{sf}) and reference state in the *green mesh* (Ω_0)

is presented showing both experimental and numerical techniques.

4.1 Initial strains model validation

A experimental value of $\lambda_0 = 1.2035$ was obtained by measuring the shortening (4.54 ± 1.325 mm) of a point located in the muscle distal end along the longitudinal direction of 9 TA muscles (Ramírez et al. 2010). This effect can be observed in the superimposed image of the real muscle in Fig. 6a. When the tendon is cut, the muscle-tendon unit suffers a great change in its geometry to achieve a stress-free configuration.

Initial strains were numerically implemented in terms of a initial deformation gradient assuming a uniform distribution in the whole muscle. In this way, the shortening in the fibre direction was used to determine the initial deformation gradient (Eq. 9).

Figure 6b represents the external geometry variation of the finite element mesh under these initial strain effects. The constraint of the distal nodes is removed after applying the deformation gradient $\mathbf{F}_0$ (Eq. 10) simulating the cut-off tendon.

4.2 Passive behaviour validation

The finite element mesh of the TA muscle was subjected to immobilisation for all degrees of freedom in the proximal region nodes and to an imposed displacement of 10 mm in the distal region (nodes at the end of the tendon). This configuration corresponds to the tensile test of the whole muscle-tendon unit described by Calvo et al. (2010). Experimental tensile tests were performed with the distal tendon cut-off, so the numerical simulation starts in the stress-free configuration (Ω_{sf}). The experimental set-up and the numerical simulation are presented in Fig. 7. In this figure, the same external configuration of the stretched muscle can be observed both in the experimental test and the numerical model.

Figure 8 represents the mean load-displacement relation (MTR-mean) obtained in the experimental test. In this figure, the results of four different numerical simulations are shown. These simulations have been performed using different constitutive parameters of the material model behaviour and fibre orientation. The first simulation (Numerical 1) was performed considering muscle and tendon material model parameters as the mean of those of various experimental tests

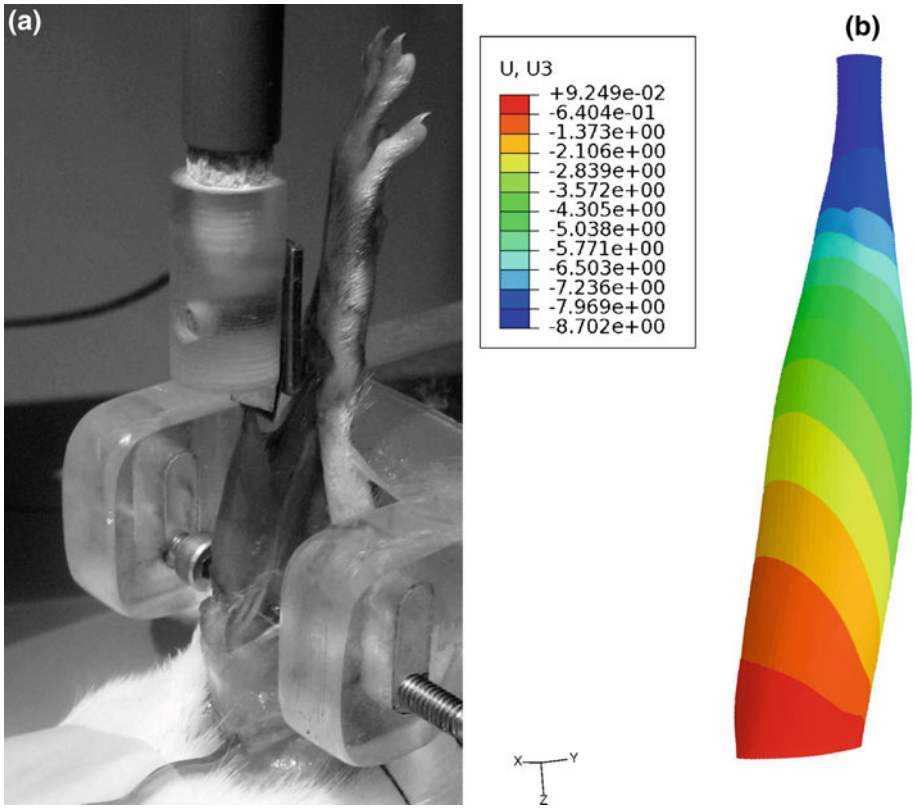

Fig. 7 Imposition of boundary conditions: **a** experimental test, **b** displacement solution

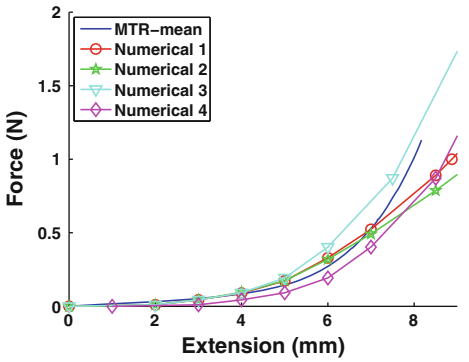

Fig. 8 Experimental mean tensile test result versus numerical simulations. MTR-mean: Mean relation obtained from experimental test. Numerical 1: Muscle and Tendon material parameters obtained from Table 1 ($\text{Muscle}_{\text{mean parameters}}$ and $\text{Tendon}_{\text{mean parameters}}$) fibres oriented in the same longitudinal direction. Numerical 2: Muscle and Tendon material parameters obtained from Table 1 ($\text{Muscle}_{\text{mean curve}}$ and $\text{Tendon}_{\text{mean curve}}$) fibres oriented in the same longitudinal direction. Numerical 3: Same material parameters as Numerical 1, fibres oriented following fusiform muscle geometry. Numerical 4: Same material parameters as Numerical 2, fibres oriented following fusiform muscle geometry

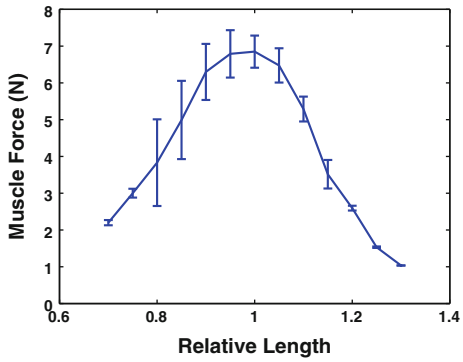

Fig. 9 Experimental force-length relation for a pulse train frequency of 60 Hz

($\text{Muscle}_{\text{mean parameters}}$ and $\text{Tendon}_{\text{mean parameters}}$ in Table 1). In this model, only one longitudinal direction is defined for fibres along the muscle length. The second numerical result (Numerical 2) considered material parameters estimated from a curve being an average of the experimental curves ($\text{Muscle}_{\text{mean curve}}$ and $\text{Tendon}_{\text{mean curve}}$ in Table 1). The same orientation was considered for muscle and tendon fibres. Simulations three and four (Numerical 3 and Numerical 4) used the same material characteristics as the previous simulations but the fibre orientation was different. In this model, the fibres for both muscle and tendon were oriented following the outline of fusiform muscle geometry.

4.3 Active behaviour validation

Figure 9 represents the mean and standard deviation of the force length relationship for TA active force obtained from "in vivo" experimental tests ($n = 6$) (Ramírez et al. 2010).

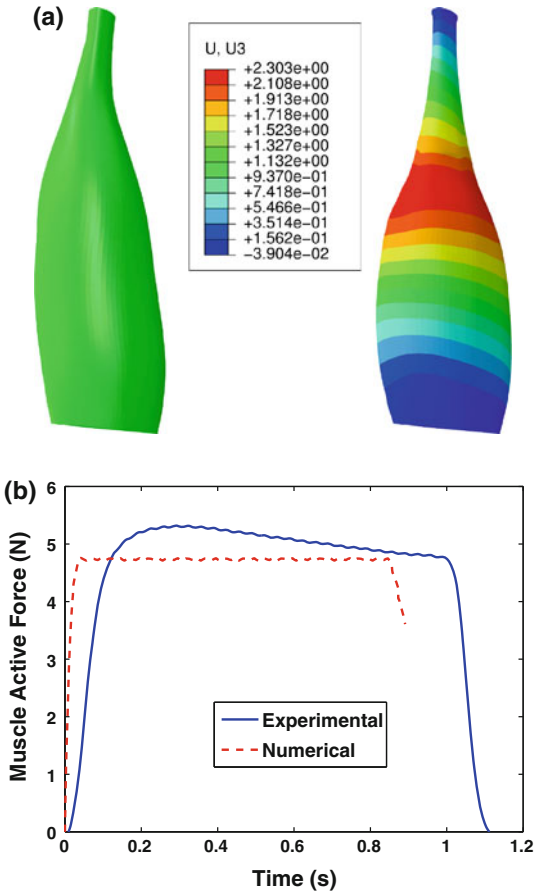

Fig. 10 **a** Initial configuration of muscle and longitudinal displacement field under isometric tenanic contraction. **b** Numerical muscle reaction force and experimental active force

As can be observed, the muscle applied its maximum force (6.85 N) at the optimal length ($\lambda = 1$).

In Fig. 10a, the undeformed geometry of the muscle is presented together with the deformed shape under isometric contraction. In this configuration, the displacement field along the longitudinal direction is plotted. Figure 10b represents the reaction force at the end of the mesh during simulation time. In this figure, the force registered by the testing machine to maintain a constant muscle length during contraction is also represented.

5 Conclusions

In this work, we have developed and validated a three-dimensional finite element model of mammalian skeletal muscle. This numerical model is capable of simulating tissue behaviour in healthy conditions incorporating both passive and active isometric contractions.

Most numerical models in the literature for skeletal muscle simulation reconstruct the geometry of specific muscle from cadavers (d'Aulignac et al. 2005; Böl and Reese 2008) or use idealized muscle geometry (Tsui et al. 2004; Blemker et al. 2005; Böl and Reese 2008; Tang et al. 2009). Conclusions from these studies depend on accurate representation of muscle architecture and geometry (Blemker and Delp 2005) to enhance the accuracy of musculoskeletal system models for medical applications. In this context, our model provides a real reconstruction from MR images of the rat TA muscle. This muscle has been previously modelled but under an idealized projection of the mid-sagittal plane (Oomens et al. 2003).

In order to obtain mechanical properties of this tissue, it is necessary to perform experimental studies. Such testing is not practical in humans and can be achieved more easily through the use of an animal model. "In vivo" methodologies have been developed to test active behaviour of experimental animals such as rabbits (Davis et al. 2003; Grover et al. 2007) and for rats in different hind limb muscles (Hawkins and Bey 1997; Huijing et al. 1998; Monti et al. 2003). The results from these tests are similar to those of the author's previous works (Calvo et al. 2010; Ramírez et al. 2010) but they were not performed for related numerical simulation studies.

The passive model proposed in this work presents results that are in good agreement with experimental passive behaviour of the muscle-tendon unit. The force displacement curves from experimental tests and from numerical simulations exhibit the same trend. From these curves, it can be observed that when fibres are oriented following fusiform muscle geometry, the hyperelastic model fits better the experimental curve for large displacements. This has been previously pointed out by Tang et al. (2009) in their analysis of stress fields inside an idealized frog gastrocenemius muscle, in which they concluded that it is necessary to consider fibre orientation when modelling these type of muscles.

The numerical model considers initial strains that, as far as the authors know, have never been considered in this way for muscle tissue. As previously mentioned, to enhance the accuracy of models obtained by MRI, this consideration is very important. The shortening of the muscle model due to its initial strains has been validated with experimental observations. It is important to note that the principal limitation of this model is the fact that a uniform deformation gradient has been considered. Finite element simulations subjecting the mesh nodes to imposed displacement, validated with a carefully image analysis of the muscle in the different configurations (initial and current), could improve this limitation.

The deformed model geometry under isometric contraction agrees well with the experimental observation of the rat TA muscle. Force generated by the muscle "in vivo" is also reproduced by the numerical model obtaining the same average value of active force. The limitations of the model are the consideration of the same type of muscular fibres in the whole muscle and that all fibres contract isometrically. The latter implies that fixing muscle ends does not guarantee that

fibres inside the muscle belly are under isometric conditions. This is a consequence of a series of elastic component elongations leading to shortening and re-lengthening of active muscle components. The main difference is observed in the load decreasing during tetanus in the experimental curve. This effect, studied in detail by Ramírez et al. (2010) and also observed by others (Hawkins and Bey 1997), was not considered in this work.

Acknowledgments The authors gratefully acknowledge research support from the Spanish Ministry of Science and Technology through the research projects DPI2008-02335, DPI2009-14115-C03-01 and grant PI071133 from the "Fondo de Investigación Sanitaria of Spain" The authors also wish to thank the Tissue Characterisation Platform of CIBER-BBN for their technical support during the experimental tests. CIBER-BBN is an initiative funded by the VI National R&D&i Plan 2008–2011, Iniciativa Ingenio 2010, Consolider Program, CIBER Actions and financed by the Instituto de Salud Carlos III with assistance from the European Regional Development Fund.

References

Arruda EM, Mundy K, Calve S, Baar K (2007) Denervation does not change the ratio of collagen i and collagen iii mrna in the extracellular matrix of muscle. Am J Physiol Regul Integr Comp Physiol 292(2):R983–R987

Blemker BB, Delp SL (2005) Three-dimensional representation of complex muscle architectures and geometries. Ann Biomed Eng 33:661–673

Blemker BB, Pinsky PM, Delp SL (2005) A 3d model of muscle reveals the causes of nonuniform strains in the biceps brachii. Ann Biomed Eng 38:657–665

Böl M, Reese S (2008) Micromechanical modelling of skeletal muscles based on the finite element method. Comput Methods Biomech Biomed Engin 11:489–504

Borg TK, Caulfield JB (1980) Morphology of connective tissue in skeletal muscle. Tissue Cell 12(1):197–207

Calvo B, Ramírez A, Alonso A, Grasa J, Soteras F, Osta R, Muñoz MJ (2010) Passive nonlinear elastic bechaviour of skeletal muscle: experimental results and model formulation. J Biomech 43:318–325

Chi S-W, Hodgson J, Chen JS, Reggie Edgerton V, Shin DD, Roiz RA, Sinha S (2010) Finite element modeling reveals complex strain mechanics in the aponeuroses of contracting skeletal muscle. J Biomech 43(7):1243–1250

d'Aulignac D, Martins JA, Pires EB, Mascarenhas T, Jorge RM (2005) A shell finite element model of the pelvic floor muscles. Comput Methods Biomech Biomed Engin 8(5):339–347

Davis J, Kaufman KR, Lieber RL (2003) Correlation between active and passive isometric force and intramuscular pressure in the isolated rabbit tibialis anterior muscle. J Biomech 36(4):505–512

Fernandez JW, Buist ML, Nickerson DP, Hunter PJ (2005) Modelling the passive and nerve activated response of the rectus femoris muscle to a flexion loading: a finite element framework. Med Eng Phys 27(10):862–870

Fernandez JW, Hunter PJ (2005) An anatomically based patient-specific finite element model of patella articulation: towards a diagnostic tool. Biomech Model Mechanobiol 4(1):20–38

Gardiner JC, Weiss JA (2003) Subject-specific finite element analysis of the human medial collateral ligament during valgus knee loading. J Orthop Res 21(6):1098–1106

Gardiner JC, Weiss JA, Rosenberg TD (2001) Strain in the human medial collateral ligament during valgus lading of the knee. Clin Orthop Relat Res 391:266–274

Grover JP, Corr DT, Toumi H, Manthei D, Oza AL, Vanderby R, Best TM (2007) The effect of stretch rate and activation state on skeletal muscle force in the anatomical range. Clin Biomech (Bristol, Avon) 22(3):360–368

Hawkins D, Bey M (1997) Muscle and tendon force-length properties and their interactions in vivo. J Biomech 30(1):63–70

Hibbit K, Sorensen (2006) Abaqus user's guide, v. 6.5. HKS inc. Pawtucket, RI USA. http://www.simulia.com/

Hill AV (1938) The heat of shortening and the dynamic constants of muscle. In: Proceedings of the royal society of London. Series B, Biological Sciences 126, pp 136–195

Holzapfel GA (2000) Nonlinear solid mechanics. A continuum approach for engineering. Wiley, London

Huijing PA, Baan GC, Rebel GT (1998) Non-myotendinous force transmission in rat extensor digitorum longus muscle. J Exp Biol 201(Pt 5):683–691

Johansson T, Meier P, Blickhan R (2000) A finite-element model for the mechanical analysis of skeletal muscles. J Theor Biol 206(1):131–149

MacIntosh BR, Gardiner PF, McComas AJ (2006) Skeletal muscle form and function, 2nd edn. Human Kinetics

Magid A, Law DJ (1985) Myofibrils bear most of the resting tension in frog skeletal muscle. Science 230(4731):1280–1282

Martins JAC, Pires EB, Salvado R, Dinis PB (1998) Numerical model of passive and active behavior of skeletal muscles. Comput Methods Appl Mech Eng 151:419–433

Materialise (2010) Mimics. Materialise Medical Software. http://www.materialise.com/mimics

Monti RJ, Roy R, Zhong H, Edgerton VR (2003) Mechanical properties of rat soleus aponeurosis and tendon during variable recruitment in situ. J Exp Biol 206(Pt 19):3437–3445

Oomens CWJ, Maenhout M, van Oijen CH, Drost MR, Baaijens FP (2003) Finite element modelling of contracting skeletal muscle. Philos Trans R Soc Lond B Biol Sci 358(1437):1453–1460

Peña E, Martinez MA, Calvo B, Doblaré M (2006) On the numerical treatment of initial strains in biological soft tissues. Int J Numer Methods Eng 68(8):836–860

Ramírez A, Grasa J, Alonso A, Soteras F, Osta R, Muñoz MJ, Calvo B (2010) Active response of skeletal muscle. In vivo experimental results and model formulation. J Theor Bio 267:546–553

Tang CY, Zhang G, Tsui CP (2009) A 3d skeletal muscle model coupled with active contraction of muscle fibres and hyperelastic behaviour. J Biomech 42(7):865–872

Tsui CP, Tang CY, Leung CP, Cheng KW, Ng YF, Chow DH, Li CK (2004) Active finite element analysis of skeletal muscle-tendon complex during isometric, shortening and lengthening contraction. Biomed Mater Eng 14:271–279

Weiss JA, Maker BN, Govindjee S (1996) Finite element implementation of incompressible, transversely isotropic hyperelasticity. Comput Methods Appl Mech Eng 135:107–128

Yucesoy CA, Koopman BHFJM, Huijing PA, Grootenboer HJ (2002) Three-dimensional finite element modeling of skeletal muscle using a two-domain approach: linked fiber-matrix mesh model. J Biomech 35(9):1253–1262